Material Modeling and Microstructural Optimization of Dielectric Elastomer Actuators

M. Klassen, B. X. Xu, S. Klinkel and R. Müller

The modeling and 3D numerical implementation of dielectric elastomer actuators are discussed in this work. The electromechanical coupling for the actuator is realized via the Maxwell stress in the mechanical balance. In this nonlinear numerical problem the consistent tangent matrix, which is used for the Newton iterations, is described in detail. The operational curve of a homogeneous capacitor structure is compared to analytical solutions by implementing the Neo-Hooke and the Yeoh material model in the numerical simulations respectively. In this simulations the instability aspects of this type of structure is discussed. Furthermore the optimization of the operational curve is analyzed for both material models through the consideration of inclusion materials in the elastomer structure. Piezoceramic and a soft material inclusions with a fiber and a spherical geometry are considered. The results show the capability of improving the operational curves of the actuator with these inhomogeneities.

1 Introduction

In the field of sensor and actuator design, dielectric elastomer actuators (DEAs) have captured the attention in the last years. Analogously to piezoceramic materials, dielectric elastomers can be deformed through the application of an electric field. One of the main differences with respect to piezoceramics is the deformation and force range of DEAs. While piezoceramics can achieve large forces with small deformations, DEAs achieve deformations and forces which lie in the range of natural muscles. For this reason one of the main application fields of DEAs is robotics where they are used as actuators for large deformations.

In this work a numerical framework for the simulation of DEAs is first presented. In reference to the previous formulations for dielectric elastomers, e.g. Dorfmann and Ogden (2005), Dorfmann and Ogden (2006), Dorfmann and Ogden (2010), McMeeking and Landis (2005) and Vu et al. (2007), a formulation starting from the actual configuration is given in this work. For more detailed and fundamental literature on the definition of the Maxwell stress, the reader is referred to the publications of Eringen (1963), Pao (1978), Toupin (1956) and Maugin et al. (1992). One aspect that is emphasized in this work is the numerical implementation. Here the derivatives which are necessary to set up the tangent matrix are described in detail.

After the introduction of the numerical background an analysis of the microstructure of DEAs is performed in the context of the finite element analysis. In this analysis, the aim is to study the influence of inclusion materials on the compression behavior of DEAs. As an extension of the previous work (Mueller et al., 2010), this work is denoted to 3D modeling and implementation with additional mechanical models (the Yeoh). Since only the microstructure of the material is considered in these examples, the influence of the surrounding free space is neglected. It should be noted, that for other application cases the surrounding free space can be considered like for example in (Vu and Steinmann, 2009). Finally this paper comes to the end with concluding remarks of the obtained results.

2 Nonlinear Electromechanics

The fundamental equations to describe the nonlinear kinematics and the electromechanical balance are introduced here. Furthermore the constitutive ingredients are presented for this type of problem. To close the section, a numerical implementation strategy is formulated which allows an implementation in the finite element method. Thereby the derivation of the tangent matrix is described in detail.

2.1 Basic Equations

In the nonlinear context a reference configuration $\mathcal{B}_0$ of a material body is considered in which the position of a point is addressed by the vector $\boldsymbol{X}$. The deformed or actual configuration is denoted by $\mathcal{B}$. The position of a material point $\boldsymbol{x}$ in the actual configuration is mapped from the reference configuration with the mapping $\boldsymbol{x} = \chi(\boldsymbol{X})$. The deformation gradient is

$$\boldsymbol{F} = \frac{\partial \boldsymbol{x}}{\partial \boldsymbol{X}}, \tag{1}$$

with the determinant of the deformation gradient $\boldsymbol{F}$, denoted by J.

$$J = \det \boldsymbol{F}. \tag{2}$$

Proper deformation measures are defined by the right and left Cauchy-Green tensor which are

$$\boldsymbol{C} = \boldsymbol{F}^T \boldsymbol{F} \quad \text{and} \quad \boldsymbol{b} = \boldsymbol{F} \boldsymbol{F}^T, \tag{3}$$

or the Green-Lagrange strain tensor which is given as

$$\boldsymbol{G} = \frac{1}{2}(\boldsymbol{F}^T \boldsymbol{F} - \mathbf{1}) = \frac{1}{2}(\boldsymbol{C} - \mathbf{1}). \tag{4}$$

The electric field quantities are described in the actual configuration by the use of the variables $\boldsymbol{D}$ and $\boldsymbol{E}$. The variable $\boldsymbol{D}$ is the electric displacement or the induction vector, while $\boldsymbol{E}$ is the vector of the electric field. For the sake of simplicity, the absence of a magnetic field and free volume charges are assumed. Furthermore, electrostatic conditions are assumed, thus the electric field is free of rotations. With this assumptions Maxwell's equations reduce to

$$\text{div} \boldsymbol{D} = 0 \tag{5}$$

and

$$\text{curl} \boldsymbol{E} = \mathbf{0} \longleftrightarrow \boldsymbol{E} = -\text{grad}\varphi. \tag{6}$$

Since the electric field is rotation free it can be defined as the gradient of the electric potential φ. In a dielectric material the electric displacement caused by an electric field is described through the equation

$$\boldsymbol{D} = \kappa_0 \boldsymbol{E} + \boldsymbol{P}. \tag{7}$$

Herein $\boldsymbol{P}$ defines the electric polarization density of the material and κ_0 is the permittivity of free space.
In the mechanical balance the external volume forces are neglected for the sake of simplicity. The equilibrium condition is written in the actual configuration as

$$\text{div}\boldsymbol{\sigma} + \boldsymbol{f}^E = \mathbf{0}, \tag{8}$$

where $\boldsymbol{f}^E$ represents the electrostatic volume force and $\boldsymbol{\sigma}$ the Cauchy stress. The electrostatic volume force can be regarded as the divergence of the so called Maxwell stress $\boldsymbol{\sigma}^E$

$$\boldsymbol{f}^E = \text{div}\boldsymbol{\sigma}^E. \tag{9}$$

By using this definition of the electrostatic volume force, the mechanical balance equation (8) is written in a compact form where the total stress $\boldsymbol{\tau}$ is composed by the sum of the Cauchy stress and the Maxwell stress,

$$\text{div}(\boldsymbol{\sigma} + \boldsymbol{\sigma}^E) = \text{div}\boldsymbol{\tau} = \mathbf{0}. \tag{10}$$

The Maxwell stress, which describes the interaction of electric forces and mechanical momentum, is defined as a function of the electrostatic fields $\boldsymbol{E}$ and $\boldsymbol{D}$ and the permittivity of vacuum κ_0 via

$$\boldsymbol{\sigma}^E = \boldsymbol{E} \otimes \boldsymbol{D} - \frac{1}{2}\kappa_0(\boldsymbol{E} \cdot \boldsymbol{E})\mathbf{1}. \tag{11}$$

Considering this definition of the Maxwell stress and by definition (9) the electrostatic volume force turns out to be

$$\boldsymbol{f}^E = (\text{grad}\boldsymbol{E})^T \boldsymbol{P} = (\text{grad}\boldsymbol{E})\boldsymbol{P}. \tag{12}$$

This volume force can be interpreted as the force per volume of the actual configuration on a dipole density.

2.2 Constitutive Laws

In addition to the governing field equations, constitutive laws for the total stress $\boldsymbol{\tau}$ and the material polarization $\boldsymbol{P}$ are needed to complete the formulation of nonlinear electromechanical deformations. In this context the conservation of mass is defined by the relation of the densities in the reference and current configuration

$$\rho_0 = J\rho. \tag{13}$$

The polarization is obtained in the actual configuration as a function of the material density

$$\boldsymbol{P} = \frac{\kappa_0 \kappa_r}{J} \boldsymbol{E}, \tag{14}$$

where κ_r is the relative permittivity of the dielectric material. With this relationship between the polarization and the electric field the electric displacement is defined by means of equation (7) in the current configuration by

$$\boldsymbol{D} = \kappa_0 (1 + \frac{\kappa_r}{J}) \boldsymbol{E}. \tag{15}$$

For the numerical implementation in the reference configuration the electric displacement has to be pulled back to the reference configuration. The pull back operation

$$\boldsymbol{D}_0 = J \boldsymbol{F}^{-1} \boldsymbol{D}, \tag{16}$$

yields the electric displacement

$$\boldsymbol{D}_0 = \kappa_0 (J + \kappa_r) \boldsymbol{C}^{-1} \boldsymbol{E}_0, \tag{17}$$

where $\boldsymbol{E}_0$ is the electric field in the reference configuration given by $\boldsymbol{E}_0 = \boldsymbol{F}^T \boldsymbol{E}$. Additionally, the Maxwell stress tensor, which was introduced in equation (11), can also be pulled back to the reference configuration by a proper pull back operation yielding

$$\boldsymbol{S}_0^E = (\boldsymbol{C}^{-1} \boldsymbol{E}_0) \otimes \boldsymbol{D}_0 - \frac{1}{2} \kappa_0 J \left[\boldsymbol{E}_0 \cdot (\boldsymbol{C}^{-1} \boldsymbol{E}_0) \right] \boldsymbol{C}^{-1}. \tag{18}$$

So far only the constitutive relations for the electric part have been considered. In this work, two material models are considered, namely the Neo-Hooke and the Yeoh model. The first model has been chosen for the reason that it is a widely used model in numerical mechanics. The second one, the Yeoh model, has been taken into account because it can describe the behavior of rubber-like materials more accurately for large deformations. For the compressible Neo-Hooke model the stress is given as a function of the left Cauchy-Green stain tensor $\boldsymbol{b}$ by

$$\boldsymbol{\sigma}^{NH} = \frac{\lambda}{2J} (J^2 - 1) \mathbf{1} + \frac{\mu}{J} (\boldsymbol{b} - \mathbf{1}) \tag{19}$$

where μ and λ are the Lamé parameters. For the compressible Yeoh model, the stress is defined as

$$\boldsymbol{\sigma}^Y = 2J^{-\frac{5}{3}} h \boldsymbol{b} + \left[-\frac{2}{3} I_1 J^{-\frac{5}{3}} h + 2c_{11}(J - 1) \right] \mathbf{1}, \tag{20}$$

where

$$h = c_{10} + 2c_{20}(J^{-\frac{2}{3}} I_1 - 3) + 3c_{30}(J^{-\frac{2}{3}} I_1 - 3)^2. \tag{21}$$

Here c_{10}, c_{20}, c_{30}, c_{11} are material parameters and $I_1 = \text{tr}(\boldsymbol{C})$ is the first invariant of the right Cauchy-Green tensor $\boldsymbol{C}$.

For a numerical implementation in the reference configuration, the stresses have to be pulled back. With the pull back operations the second Piola-Kirchhoff stresses for both models are obtained

$$\boldsymbol{S}_0^{NH} = \frac{\lambda}{2} (J^2 - 1) \boldsymbol{C}^{-1} + \mu (\mathbf{1} - \boldsymbol{C}^{-1}) \tag{22}$$

and

$$\boldsymbol{S}_0^Y = 2J^{-\frac{2}{3}} h \mathbf{1} + \left[-\frac{2}{3} I_1 J^{-\frac{2}{3}} h + 2c_{11} J(J - 1) \right] \boldsymbol{C}^{-1}. \tag{23}$$

2.3 Numerical Implementation

The numerical implementation in this work is done in the reference configuration. To solve the electromechanical coupled problem the weak forms of the mechanical equilibrium (10) and of Gauß' equation (5) are considered. Neglecting surface charges, the two weak forms in the reference configuration are

$$\int_{\mathcal{B}_0} (\boldsymbol{S}_0 + \boldsymbol{S}_0^E) : \delta \boldsymbol{G} dV = 0 \tag{24}$$

and

$$- \int_{\mathcal{B}_0} \boldsymbol{D}_0 \cdot \delta \boldsymbol{E}_0 dV = 0. \tag{25}$$

Herein $\delta \boldsymbol{G}$ is the Green-Lagrange strain tensor for a kinematically admissible virtual displacement and $\delta \boldsymbol{E}_0$ is a virtual electric field.

The body $\mathcal{B}_0$ is discretized with finite elements. In the context of the isoparametric concept the displacement $\boldsymbol{x}$ and the electric potential φ are discretized by the elements with linear shape functions. With this discretization the two residuals are in Voigt-notation

$$\underline{\boldsymbol{R}}_I^m(\underline{\boldsymbol{u}}_J, \varphi_J) = - \int_{\mathcal{B}_0^e} \underline{\boldsymbol{B}}_I^T (\underline{\boldsymbol{S}}_0 + \underline{\boldsymbol{S}}_0^E) dV \tag{26}$$

and

$$R_I^e(\underline{\boldsymbol{u}}_J, \varphi_J) = - \int_{\mathcal{B}_0^e} \tilde{\underline{\boldsymbol{B}}}_I^T \underline{\boldsymbol{D}}_0 dV. \tag{27}$$

Herein I are the node numbers. The matrices $\underline{\boldsymbol{B}}_I$ and $\tilde{\underline{\boldsymbol{B}}}_I$ are formed by the derivatives of the shape functions. For the 3d case the B-operators are

$$\underline{\boldsymbol{B}}_I = \begin{bmatrix} F_{11} N_{I,1} & F_{21} N_{I,1} & F_{31} N_{I,1} \\ F_{12} N_{I,2} & F_{22} N_{I,2} & F_{32} N_{I,2} \\ F_{13} N_{I,3} & F_{23} N_{I,3} & F_{33} N_{I,3} \\ F_{11} N_{I,2} + F_{12} N_{I,1} & F_{21} N_{I,2} + F_{22} N_{I,1} & F_{31} N_{I,2} + F_{32} N_{I,1} \\ F_{12} N_{I,3} + F_{13} N_{I,2} & F_{22} N_{I,3} + F_{23} N_{I,2} & F_{32} N_{I,3} + F_{33} N_{I,2} \\ F_{11} N_{I,3} + F_{13} N_{I,1} & F_{21} N_{I,3} + F_{23} N_{I,1} & F_{31} N_{I,3} + F_{33} N_{I,1} \end{bmatrix}, \quad \tilde{\underline{\boldsymbol{B}}}_I = \begin{bmatrix} N_{I,1} \\ N_{I,2} \\ N_{I,3} \end{bmatrix}. \tag{28}$$

The first residual (26) is considered as the mechanical residual and the second residual (27) is the electric residual. The nonlinear problem is solved by a Newton method. For this reason the tangent matrix has to be computed in each iteration step. In the case of the considered coupled problem the matrix is composed of four sub matrices

$$\underline{\boldsymbol{K}}_{IJ} = \begin{bmatrix} \underline{\boldsymbol{K}}_{IJ}^{mm} & \underline{\boldsymbol{K}}_{IJ}^{me} \\ \underline{\boldsymbol{K}}_{IJ}^{em} & K_{IJ}^{ee} \end{bmatrix}. \tag{29}$$

The four sub matrices are calculated through the derivation of the two residuals by the mechanical displacement and the electric potential.

$$\underline{\boldsymbol{K}}_{IJ}^{mm} = - \frac{\partial \underline{\boldsymbol{R}}_I^m}{\partial \underline{\boldsymbol{u}}_J}, \qquad \underline{\boldsymbol{K}}_{IJ}^{me} = - \frac{\partial \underline{\boldsymbol{R}}_I^m}{\partial \varphi_J}, \qquad \underline{\boldsymbol{K}}_{IJ}^{em} = - \frac{\partial R_I^e}{\partial \underline{\boldsymbol{u}}_J}, \qquad K_{IJ}^{ee} = - \frac{\partial R_I^e}{\partial \varphi_J} \tag{30}$$

The calculation of the derivatives is done in an analytical manner.

2.3.1 Derivatives for the Tangent Matrix

For the first sub matrix the mechanical residual is derived by the mechanical displacement. By applying the product rule for derivatives we obtain

$$\mathbf{K}_{IJ}^{mm} = - \frac{\partial \mathbf{R}_I^m}{\partial \underline{\mathbf{u}}_J} = \frac{\partial}{\partial \underline{\mathbf{u}}_J} \int \mathbf{B}_I^T (\mathbf{S}_0 + \mathbf{S}_0^E) dV = \int \mathbf{B}_I^T \frac{\partial (\mathbf{S}_0 + \mathbf{S}_0^E)}{\partial \underline{\mathbf{u}}_J} dV + \int \frac{\partial \mathbf{B}_I^T}{\partial \underline{\mathbf{u}}_J} (\mathbf{S}_0 + \mathbf{S}_0^E) dV, \tag{31}$$

in which the second term is the geometrical part. Considering the first term, the second Piola Kirchhoff stress $\underline{\boldsymbol{S}}_0$ and the Maxwell stress in the reference configuration $\underline{\boldsymbol{S}}_0^E$ are derived w.r.t. the displacement. For this derivatives the chain rule is applied. For the second Piola Kirchhoff stress this would be

$$\frac{\partial \mathbf{S}_0}{\partial \underline{\mathbf{u}}_J} = \frac{\partial \mathbf{S}_0}{\partial \mathbf{G}} \frac{\partial \mathbf{G}}{\partial \underline{\mathbf{u}}_J} = \frac{\partial \mathbf{S}_0}{\partial \mathbf{C}} \frac{\partial \mathbf{C}}{\partial \mathbf{G}} \frac{\partial \mathbf{G}}{\partial \underline{\mathbf{u}}_J}. \tag{32}$$

The derivative of the right Cauchy-Green tensor w.r.t. the Green-Lagrange tensor is

$$\underline{\mathbf{G}} = \frac{1}{2}(\underline{\mathbf{C}} - \underline{\mathbf{1}}) \quad \rightarrow \quad \underline{\mathbf{C}} = 2\underline{\mathbf{G}} - 2\underline{\mathbf{1}} \quad \rightarrow \quad \frac{\partial \underline{\mathbf{C}}}{\partial \underline{\mathbf{G}}} = 2\mathbb{I}, \tag{33}$$

where $\mathbb{I}$ is the fourth order identity tensor in Voigt notation. The derivative of the Green-Lagrange by the displacement is obtained through the discretization of the displacement field

$$\underline{\mathbf{G}} = \sum_{J=1}^{N} \mathbf{B}_J \mathbf{u}_J \quad \rightarrow \quad \frac{\partial \underline{\mathbf{G}}}{\partial \mathbf{u}_J} = \mathbf{B}_J. \tag{34}$$

With this reformulations the derivatives of the two stresses w.r.t the displacement are

$$\frac{\partial \underline{\mathbf{S}}_0}{\partial \mathbf{u}_J} = \frac{\partial \underline{\mathbf{S}}_0}{\partial \underline{\mathbf{C}}} 2\mathbf{B}_J \quad \text{and} \quad \frac{\partial \underline{\mathbf{S}}_0^E}{\partial \mathbf{u}_J} = \frac{\partial \underline{\mathbf{S}}_0^E}{\partial \underline{\mathbf{C}}} 2\mathbf{B}_J. \tag{35}$$

For the second term, the geometrical part, the derivative is

$$\int \frac{\partial \mathbf{B}_I^T}{\partial \mathbf{u}_J}(\underline{\mathbf{S}}_0 + \underline{\mathbf{S}}_0^E)dV = \int \frac{\partial \mathbf{B}_I^T}{\partial \mathbf{u}_J}(\underline{\mathbf{T}}_0)dV = G_{IJ}\mathbb{I}, \tag{36}$$

with $\underline{\mathbf{T}}_0$ being the total stress tensor in the reference configuration, and

$$G_{IJ} = \begin{bmatrix} N_{I,1} & N_{I,2} & N_{I,3} \end{bmatrix} \begin{bmatrix} T_{11} & T_{12} & T_{13} \\ T_{21} & T_{22} & T_{23} \\ T_{31} & T_{32} & T_{33} \end{bmatrix} \begin{bmatrix} N_{J,1} \\ N_{J,2} \\ N_{J,3} \end{bmatrix}. \tag{37}$$

Finally, the first sub matrix of the tangent matrix is

$$\mathbf{K}_{IJ}^{mm} = 2 \int \mathbf{B}_I^T \left(\frac{\partial \underline{\mathbf{S}}_0}{\partial \underline{\mathbf{C}}} + \frac{\partial \underline{\mathbf{S}}_0^E}{\partial \underline{\mathbf{C}}}\right)\mathbf{B}_J dV + G_{IJ}\mathbb{I}. \tag{38}$$

For the second sub matrix, where the mechanical residual is derived w.r.t. the electric potential, one obtains

$$\mathbf{K}_{IJ}^{me} = -\frac{\partial \mathbf{R}_I^m}{\partial \varphi_J} = \frac{\partial}{\partial \varphi_J} \int \mathbf{B}_I^T(\underline{\mathbf{S}}_0 + \underline{\mathbf{S}}_0^E)dV = \int \frac{\partial \mathbf{B}_I^T}{\partial \varphi_J}(\underline{\mathbf{S}}_0 + \underline{\mathbf{S}}_0^E)dV + \int \mathbf{B}_I^T \frac{\partial(\underline{\mathbf{S}}_0 + \underline{\mathbf{S}}_0^E)}{\partial \varphi_J}dV \tag{39}$$

The first term is zero since the B-operator $\mathbf{B}_I$ is independent of the electric potential. Also the second Piola-Kirchhoff of the mechanical stress is independent of the electric potential. With this only the derivative of the Maxwell stress has to be considered. Applying the chain rule we obtain

$$\frac{\partial \underline{\mathbf{S}}_0^E}{\partial \varphi_J} = \frac{\partial \underline{\mathbf{S}}_0^E}{\partial \underline{\mathbf{E}}_0} \frac{\partial \underline{\mathbf{E}}_0}{\partial \varphi_J}. \tag{40}$$

For the derivative of the electric field by the electric potential the discretization of the electric field is considered

$$\underline{\mathbf{E}}_0 = -\sum_{J=1}^{N} \tilde{\mathbf{B}}_J \varphi_J \quad \rightarrow \quad \frac{\partial \underline{\mathbf{E}}_0}{\partial \varphi_J} = -\tilde{\mathbf{B}}_J. \tag{41}$$

With this the second sub matrix of the tangent matrix is

$$\mathbf{K}_{IJ}^{me} = -\int \mathbf{B}_I^T \frac{\partial \underline{\mathbf{S}}_0^E}{\partial \underline{\mathbf{E}}_0} \tilde{\mathbf{B}}_J dV. \tag{42}$$

For the last two sub matrices the electric residual is derived by the mechanical displacement and the electric potential. The derivative by the mechanical displacement is

$$\mathbf{K}_{IJ}^{em} = -\frac{\partial \mathbf{R}_I^E}{\partial \mathbf{u}_J} = \frac{\partial}{\partial \mathbf{u}_J} \int \tilde{\mathbf{B}}_I^T \mathbf{D}_0 dV. \tag{43}$$

Here the B-operator $\tilde{\underline{\mathbf{B}}}_I$ is independent of the mechanical displacement. To derive the electric displacement by the mechanical displacement the chain rule which was used in the first sub matrix is used again leading to

$$\frac{\partial \mathbf{D}_0}{\partial \underline{\mathbf{u}}_J} = 2 \frac{\partial \mathbf{D}_0}{\partial \underline{\mathbf{C}}} \mathbf{B}_J. \tag{44}$$

With this, the third sub matrix turns out to be

$$\underline{\mathbf{K}}_{IJ}^{em} = 2 \int \tilde{\underline{\mathbf{B}}}_I^T \frac{\partial \mathbf{D}_0}{\partial \underline{\mathbf{C}}} \mathbf{B}_J dV. \tag{45}$$

The fourth sub matrix is

$$\mathbf{K}_{IJ}^{ee} = -\frac{\partial \mathbf{R}_I^E}{\partial \varphi_J} = \frac{\partial}{\partial \varphi_J} \int \tilde{\underline{\mathbf{B}}}_I^T \mathbf{D}_0 dV. \tag{46}$$

With the application of the chain rule the derivative of the electric displacement by the electric potential is

$$\frac{\partial \mathbf{D}_0}{\partial \varphi_J} = \frac{\partial \mathbf{D}_0}{\partial \underline{\mathbf{E}}_0} \frac{\partial \underline{\mathbf{E}}_0}{\partial \varphi_J} = -\frac{\partial \mathbf{D}_0}{\partial \underline{\mathbf{E}}_0} \tilde{\mathbf{B}}_J. \tag{47}$$

Which leads to the forth sub matrix as

$$\mathbf{K}_{IJ}^{ee} = -\int \tilde{\underline{\mathbf{B}}}_I^T \frac{\partial \mathbf{D}_0}{\partial \underline{\mathbf{E}}_0} \tilde{\underline{\mathbf{B}}}_J dV. \tag{48}$$

For more details on the remaining derivatives the reader is referred to the Appendix.

3 Results

3.1 Homogeneous Capacitor

In a first step the simple geometry of a sandwich structure which is shown in Figure 1 is considered. The elastomer material lies between two compliant electrodes. By the application of a potential difference $\Delta\varphi$ on the electrodes an electric field is induced on the elastomer material. Due to the polarization of the material and the resulting Maxwell stress the sandwich structure is compressed in the direction of the electric field. The dimensions of the considered sandwich geometry are $L_x = L_y = L_z = L = 20\mu m$.
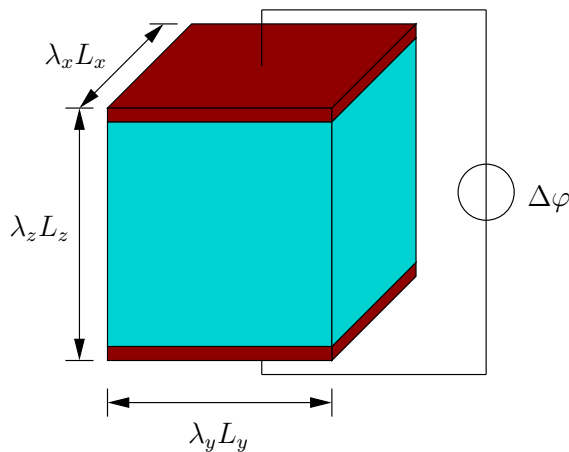

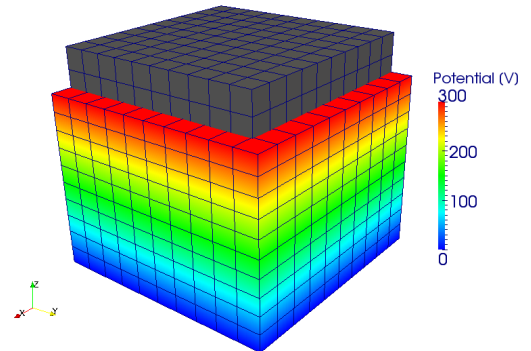Figure 1: Sandwich structure.

Figure 2: Deformation of the homogeneous sandwich structure. Neo-Hooke model.

For the numerical implementation the elastomer geometry is discretized by 1000 isoparametric solid elements with 8 nodes, see Figure 2. The electric loading is applied as a boundary condition where the electric potential φ on the upper face ($z = L$) is $300V$, and on the lower face ($z = 0$) we prescribe $\varphi = 0V$. Homogeneous boundary displacement conditions are applied on the faces $x = 0$, $y = 0$ and $z = 0$ in the respective directions. The material

is modeled by a Neo-Hooke model with the parameters $\lambda = 3.288 \cdot 10^6 N/m^2$ and $\mu = 0.4356 \cdot 10^5 N/m^2$. The relative permittivity κ_r is 7. With this parameters the elastomer model is almost incompressible, $\nu = 0.49$.

In Figure 2 it is shown that the material contracts in the z-direction and expands in the x- and y-directions under the electric loading. With the applied potential the displacement u_z of the upper face of the structure is $-3.6 \cdot 10^{-6} m$. This corresponds to a compression of about 18%.

So far only the deformation of the structure has been calculated using a Neo-Hook material model. To check if the implementation is correct an analytical solution of the deformation behavior needs to be taken into consideration. Analytical studies for this type of problem are described in e.g. (Xu et al., 2010) and (Zhao and Suo, 2007). In those two works also stability aspects for several material models have been analyzed. In our present work the Neo-Hooke and the Yeoh model are compared to the analytical findings of the cited publications. For the Neo-Hooke model the previously mentioned parameters are used again. For the Yeoh model the parameters are $c_{10} = 0.3 \cdot 10^6 N/m^2$, $c_{20} = -0.3 \cdot 10^5 N/m^2$, $c_{30} = 0.3 \cdot 10^4 N/m^2$ and $c_{11} = 1.0 \cdot 10^{12} N/m^2$. The parameter c_{11} is set to a high value to model a nearly incompressible behavior.

In Figure 3 the analytical and numerical solution are represented for both material models. The compression phenomena of the structure can be seen as a 1D problem since the compression and the application of the electric field take place along the z-axis. For this reason the normalized nominal electric field is plotted as a function of the stretch λ_z. The first curve represents the analytical solution for the equilibrium of the structure. As the electric field increases the compression also increases starting at $\lambda_z = 1$. The second curve represents the stability curve for the analytical solution. As long as the stability curve is above the equilibrium curve, the equilibrium is stable. The stability curve intersects the equilibrium curve at the point where the equilibrium curve has extreme values. These are the critical points, where the equilibrium changes from stable to unstable and vice versa. In the case of the Neo-Hooke model there is only one critical point at $\lambda_z = 0.63$ which corresponds to a compression of 37%. So for this model the equilibrium is stable as long as the compression stays below 37%. For the Yeoh model, there are two critical points which are at $\lambda_z^1 = 0.257$ and $\lambda_z^2 = 0.681$. Between these points the equilibrium is unstable. The electric field is increased until the structure is compressed by $31, 9\%$. If the electric field continues to increase at this point, the compression instantaneously jumps to the equilibrium point in the second stability range for the corresponding nominal electric field.

The third curve shows the results of the numerical implementation for both models. Both solutions coincide very well in the regions where the equilibrium is stable. As the electric field approaches the critical points, the Newton iteration in the simulation diverges. So the numerical representation of the electromechanical instability is the divergence of the Newton iteration.
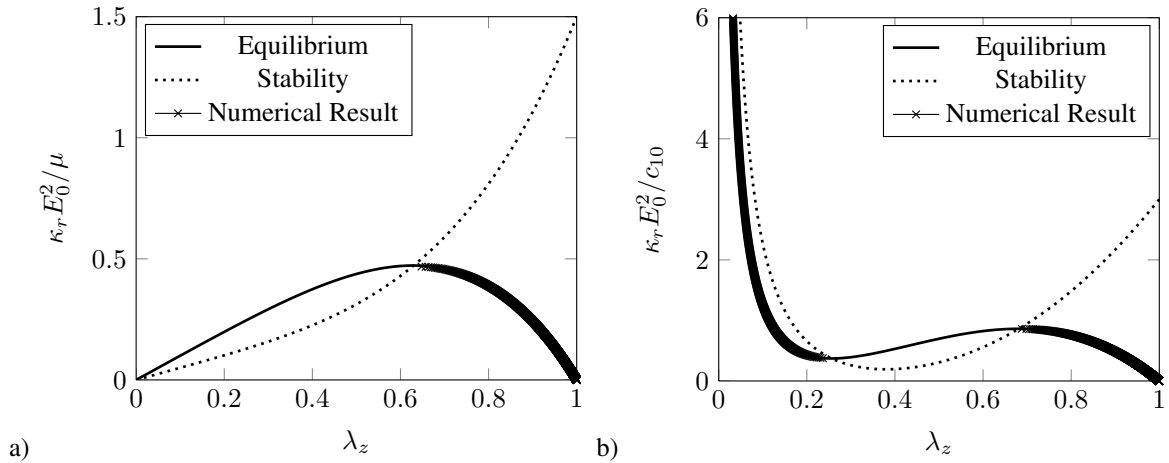

Figure 3: Analytical and numerical compression curves for a) the Neo-Hooke model and b) the Yeoh model, see (Xu et al., 2010).

3.2 Microstructural Inclusions

In this section numerical studies are performed to analyze the electromechanical behavior of an elastomer with material inclusions. Two geometry situations are considered here: a fiber inclusions modeled as cylinders and a spherical inclusion. From the material point of view also two ideas are proposed. On the one hand BaTiO$_3$, which is a known piezoceramic, is considered since the relative permittivity of this material is very high which should lead to a good electromechanical coupling. The disadvantage of this inclusion material is the high stiffness which will lead to smaller deformations. On the other hand, soft materials, for example air, are considered. The advantage

of a soft material is the low stiffness which favors large deformations. The disadvantage is the also low relative permittivity which is usually close to 1.

3.2.1 3D Fiber Inclusion

In the first case a 3d fiber inclusion is modeled as a cylinder in the sandwich structure as shown in Figure 4. The dimensions of the structure are the same as the ones mentioned in section 3.1 with a fiber diameter D of $10\mu m$.
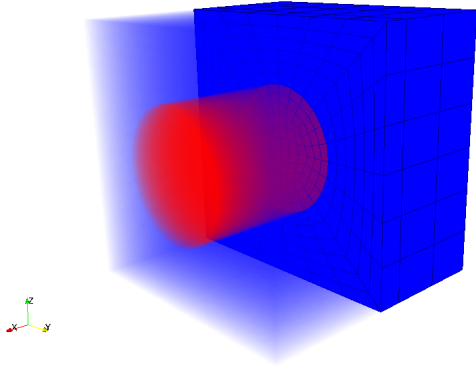

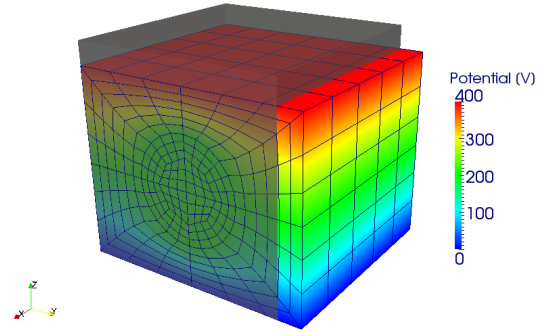
Figure 4: Geometry and mesh of the sandwich structure with fiber inclusion.

Figure 5: Deformation of the sandwich structure with fiber inclusion.

For the first numerical simulation a potential difference of $\Delta\varphi = 400V$ is applied as a boundary condition on the upper and lower face of the structure. The resulting nominal electric field for this loading and geometry is $E_0 = 20V/\mu m$. The displacements on the faces $x = 0$, $y = 0$ and $z = 0$ are set to zero in the respective directions. Furthermore the displacement on the face $x = L$ is also constrained in x-direction. Since this geometric model is considered as a microstructure, the displacement directions y and z on the faces $y = L$ and $z = L$ are linked together to enforce a constant displacement of the respective faces. The material model taken into account in this example is the Neo-Hooke model with the same parameters as presented in section 3.1 for the elastomer material. For the BaTiO$_3$ fiber also the Neo-Hooke model is considered with the parameters $\lambda = 7.42\cdot10^{10}N/m^2$, $\mu = 3.38 \cdot 10^{10}N/m^2$ and $\kappa_r = 2000$. In Figure 5, the structure is compressed in z-direction and stretched in y-direction as expected. From the distribution of the electric potential φ one can see, that the electric field is inhomogeneous. In the region of the inclusion the electric potential stays relatively constant compared to the surrounding elastomer.
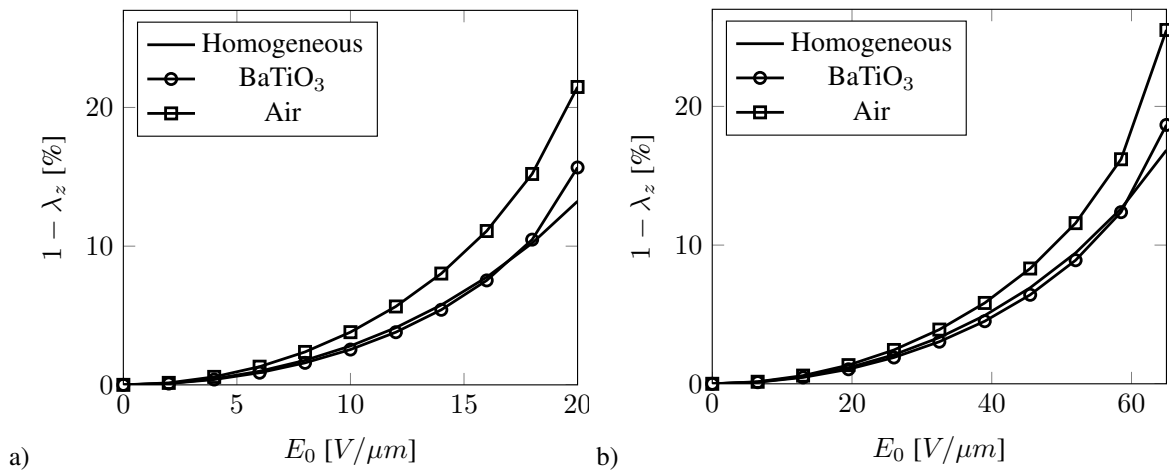

Figure 6: Compression curves for different fiber materials with constant radius for a) the Neo-Hooke model, $D = 12\mu m$ and b) the Yeoh model, $D = 10\mu m$.

For a more detailed analysis both material models are considered to model the elastomer material. As an inclusion material not only the piezoceramic but also a soft material e.g. air is considered. The soft inclusion is modeled

with the Neo-Hooke parameters $\lambda = 3.288 N/m^2$, $\mu = 6.72 \cdot 10^1 N/m^2$ and $\kappa_r = 1$ and the piezoceramic by the parameters mentioned before.

In the case of the Neo-Hooke model the diameter D of the fiber is $12 \mu m$ and the electric potential is increased through several loading steps from 0 to $400V$. For the Yeoh case the inclusion diameter D is $10 \mu m$ and the electric potential is increased from 0 to $1300V$. By choosing these diameters and electric potentials the maximum compression can be produced in both cases. Figure 6 shows the compression curves as a function of the nominal electric field for both elastomer material models. In both models, the compression increases with the applied electric field. The first curve represents the compression of the structure with no inclusions. In the case of the piezoceramic inclusion, the compression is reduced in comparison to the homogeneous case for a low electric field. This can be observed for both elastomer models. Beyond a certain nominal electric field ($E_0 \approx 17V/\mu m$ for Neo-Hooke and $E_0 \approx 60V/\mu$ for Yeoh) the compression is higher in comparison to the homogeneous situation. For the case of soft material fiber the compression is higher than the homogeneous and the piezoceramic inclusion case.

To refine this analysis in a last step, the diameter of the fiber is varied to study the influence of this dimension on the compression behavior of the inhomogeneous structure. The same parameters and boundary conditions as mentioned before are used in this analysis. The diameter is varied from $D = 0 \mu m$ to $D = 20 \mu m$. Figure 7 shows the influence of the radius of the BaTiO$_3$ inclusion at different nominal electric fields. For all electric fields the increase of the diameter produces a decrease of the compression until a certain point. Depending on the applied nominal electric field there is a diameter at which the compression improves in comparison to the homogeneous case. Taking the Neo-Hooke model for example, in the case of an electric field of $E_0 = 20V/\mu m$ the optimal diameter is above $12 \mu m$. If the electric field is $E_0 = 15V/\mu m$ the diameter has to be above $14 \mu m$ to improve the compression.
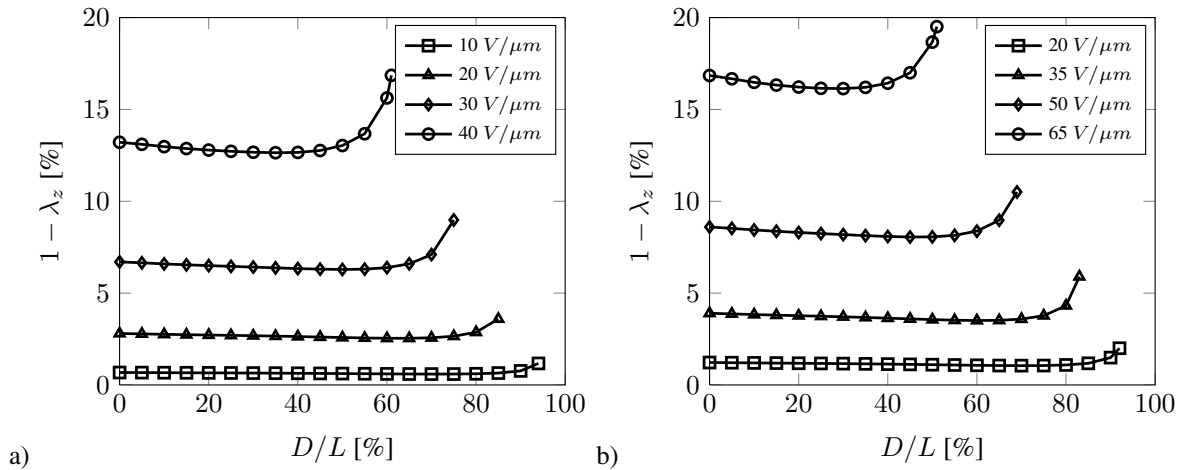

Figure 7: Compression curves with variable BaTiO$_3$ fiber radius for a) the Neo-Hooke model and b) the Yeoh model.
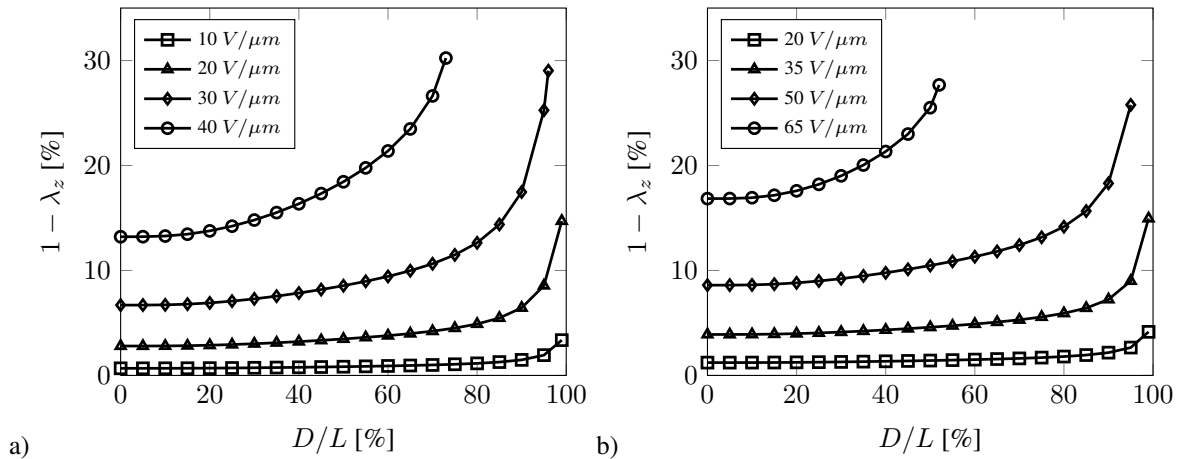

Figure 8: Compression curves with variable air fiber radius of a) the Neo-Hooke model and b) the Yeoh model.

In Figure 8 the results for soft material inclusions are presented. An increase of the inclusion produces a direct

improvement of the compression for both material models. The higher the inclusion diameter is, the higher the compression becomes.

3.2.2 3D Spherical Inclusion

In the last analysis the same settings as before are used to study the influence of a spherical inclusion on the elastomer structure, see Figure 9.
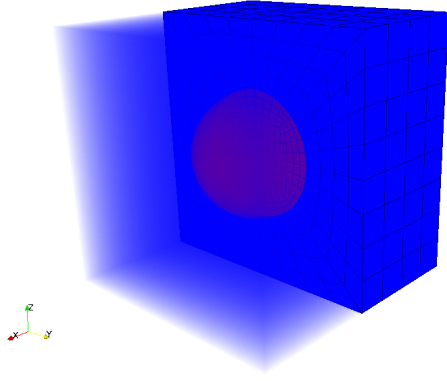

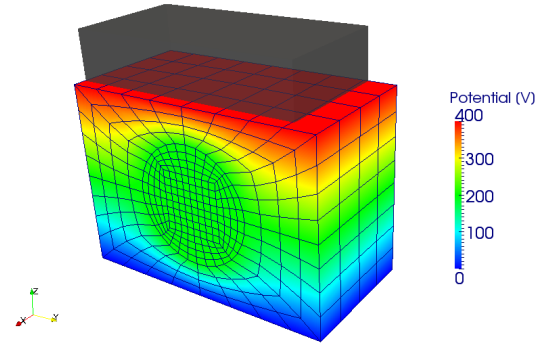Figure 9: Geometry and mesh of the sandwich structure with spherical inclusion.

Figure 10: Deformation of the sandwich structure with spherical inclusion. Cross section at $x = a/2$.

A spherical inclusion of BaTiO$_3$ with a constant diameter D of $10\mu m$ is considered in a first example. The applied potential difference is $\Delta\varphi = 400V$ and the displacement of the faces $x = 0$, $y = 0$ and $z = 0$ are constrained in the respective directions. Furthermore the displacements on the remaining faces are linked together to enforce a constant displacement of the faces since a microstructure is considered here. Figure 10 shows the region of the structure between $x = 0$ and $x = a/2$ (cut in the center). The compression and stretching of the structure can be observed as expected. Also the inhomogeneous distribution of the electric potential should be noticed. The electric field is relatively constant in the region of the spherical inclusion.

To complete the analysis the diameter of the spherical inclusion is varied between $D = 0$ and $D = 20\mu m$ for different electric loadings to show the influence of the radius on the compression. As in the case with the fiber inclusion, the optimal radius depends on the applied electric field for piezoceramic inclusions, see Figure 11. The case of soft material inclusions is omitted here, since a qualitative similar behavior as with fiber inclusions is observed.
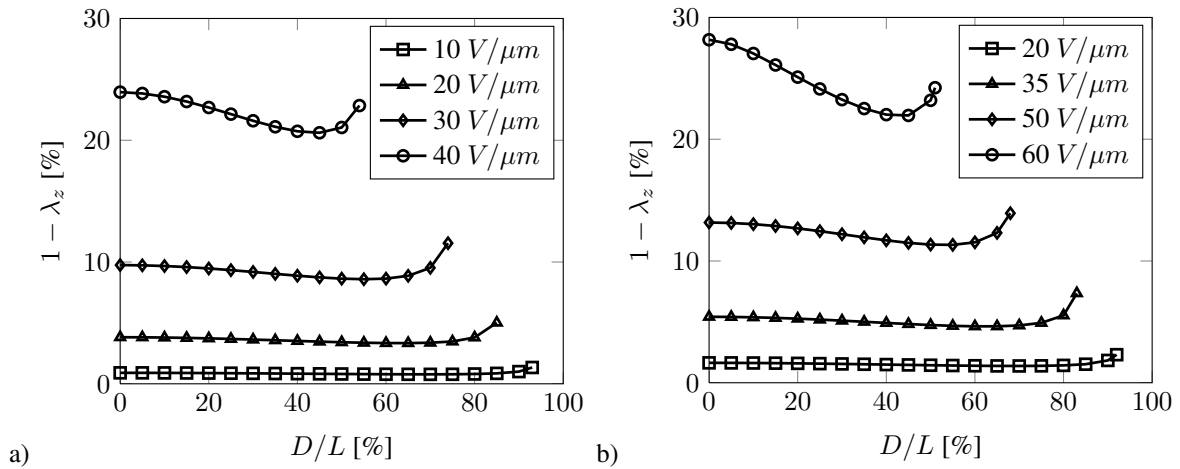

a)

b)

Figure 11: Compression curves with variable BaTiO$_3$ spherical radius for a) the Neo-Hooke model and b) the Yeoh model.

4 Conclusion

In this paper an approach for the modeling of dielectric elastomer actuators in a nonlinear context is presented. The coupling of the mechanical deformations and the electrostatic loads is done through the introduction of the Maxwell stress in the mechanical balance. For the sake of simplicity only electrostatic volume forces are considered. The required constitutive laws are presented for the electrical and the mechanical part. For the mechanical material behavior a compressible Neo-Hooke and a compressible Yeoh model are considered and compared. For the numerical implementation the coupling is realized through a symmetric tangent matrix which is composed of the analytical derivatives of the mechanical and electrical residual w.r.t. the mechanical displacement and the electric potential. As a first numerical example a homogeneous cubic elastomer structure with compliant electrodes is considered. In this example the structure is loaded with an electric potential difference leading to a nonlinear compression curve of the structure. To verify the numerical results, the compression curves of the Neo-Hooke and the Yeoh model are compared with analytical compression curves. One interesting aspect in this comparison is the instability of the elastomer structure. The instability point predicted by the analytical Neo-Hooke and Yeoh model is rendered in the numerical solution by the divergence of the Newton iterations. Furthermore the influence of inclusion materials in the elastomer structure is analyzed in this work. For this purpose fiber and spherical inclusions are contemplated with material models of the piezoceramic $BaTiO_3$ and a soft material like air. The results show that a piezoceramic inclusion material can increase the compression of the microstructure at higher electric fields. The probable reason for this phenomenon is that the electromechanical coupling takes overhand over the ceramic stiffness at a sufficient high electric field, which improves the deformation of the inhomogeneous structure. In the case of a soft inclusion with a relative permittivity of 1 the compression is increased for any electric field. In this case the stiffness of the inclusion is so low that the compression is increased even though the relative permittivity of the material do not allows a good coupling. To study the influence of the size of the inclusion the radius is varied for the mentioned inclusion cases. According to the results an optimal radius can be found for the $BaTiO_3$ material to increase the compression. This radius depends on the applied electric field. As the applied electric field gets higher a lower inclusion radius is sufficient to get an increase of the compression. In the case of air inclusions the compression increases directly in a nonlinear way with the size of the inclusion.

5 Appendix

0) Auxiliary derivatives

$$\frac{\partial J}{\partial C_{AB}} = \frac{1}{2} J C_{AB}^{-1} \tag{49}$$

$$\frac{\partial C_{AB}^{-1}}{\partial C_{CD}} = -\frac{1}{2}(C_{AC}^{-1}C_{BD}^{-1} + C_{AD}^{-1}C_{BC}^{-1}) \tag{50}$$

1) $\dfrac{\partial \underline{\mathbf{S}}_0^{NH}}{\partial \underline{\mathbf{C}}}$ (Neo-Hooke)

$$S_{0IJ}^{NH} = \frac{\lambda}{2}(J^2 - 1)C_{IJ}^{-1} + \mu(\delta_{IJ} - C_{IJ}^{-1}) \tag{51}$$

$$\frac{\partial S_{0IJ}^{NH}}{\partial C_{PQ}} = \frac{\partial}{\partial C_{PQ}}(\frac{\lambda}{2}(J^2 - 1)C_{IJ}^{-1} + \mu(\delta_{IJ} - C_{IJ}^{-1})) \tag{52}$$

$$\frac{\partial S_{0IJ}^{NH}}{\partial C_{PQ}} = \frac{\partial(\frac{\lambda}{2}(J^2 - 1))}{\partial C_{PQ}}C_{IJ}^{-1} + \frac{\lambda}{2}(J^2 - 1)\frac{\partial C_{IJ}^{-1}}{\partial C_{PQ}} + \frac{\partial(\mu(\delta_{IJ} - C_{IJ}^{-1}))}{\partial C_{PQ}} \tag{53}$$

$$\frac{\partial S_{0IJ}^{NH}}{\partial C_{PQ}} = \lambda J \frac{1}{2} J C_{PQ}^{-1} C_{IJ}^{-1} + \frac{\lambda}{2}(J^2 - 1)(-\frac{1}{2}(C_{IP}^{-1}C_{JQ}^{-1} + C_{IQ}^{-1}C_{JP}^{-1})) \tag{54}$$

$$-\mu(-\frac{1}{2}(C_{IP}^{-1}C_{JQ}^{-1} + C_{IQ}^{-1}C_{JP}^{-1}))$$

$$\frac{\partial S_{0IJ}^{NH}}{\partial C_{PQ}} = \frac{1}{2}J^2\lambda C_{IJ}^{-1}C_{PQ}^{-1} + (\frac{1}{2}\mu - \frac{1}{4}\lambda(J^2 - 1))(C_{IP}^{-1}C_{JQ}^{-1} + C_{IQ}^{-1}C_{JP}^{-1}) \tag{55}$$

2) $\dfrac{\partial \underline{\mathbf{S}}_0^{Y}}{\partial \underline{\mathbf{C}}}$ (Yeoh)

$$S_{0IJ}^{Y} = 2J^{-\frac{2}{3}}h\delta_{IJ} - \frac{2}{3}J^{-\frac{2}{3}}I_1 h C_{IJ}^{-1} + 2c_{11}(J-1)JC_{IJ}^{-1} \tag{56}$$

with

$$h = c_{10} + 2c_{20}(J^{-\frac{2}{3}}I_1 - 3) + 3c_{30}(J^{-\frac{2}{3}}I_1 - 3)^2 \tag{57}$$

The derivative of S_{0IJ}^{Y} w.r.t. C_{PQ} is written in a compact form by considering the derivative of the factor h and the derivatives of the three terms of S_{0IJ}^{Y} w.r.t. C_{PQ}.

$$\frac{\partial h}{\partial C_{PQ}} = J^{-\frac{2}{3}}(-\frac{1}{3}C_{PQ}^{-1}I_1 + \delta_{PQ})(2c_{20} + 6c_{30}(J^{-\frac{2}{3}}I_1 - 3)) \tag{58}$$

$$\frac{\partial}{\partial C_{PQ}}(2J^{-\frac{2}{3}}h1_{IJ}) = \delta_{IJ}(-\frac{2}{3}J^{-\frac{2}{3}}C_{PQ}^{-1}h + 2J^{-\frac{2}{3}}\frac{\partial h}{\partial C_{PQ}}) \tag{59}$$

$$\frac{\partial}{\partial C_{PQ}}(-\frac{2}{3}I_1 J^{-\frac{2}{3}}h C_{IJ}^{-1}) = -\frac{2}{3}(-\frac{1}{3}J^{-\frac{2}{3}}C_{PQ}^{-1}I_1 + J^{-\frac{2}{3}}\delta_{PQ})h C_{IJ}^{-1} \tag{60}$$

$$-\frac{2}{3}I_1 J^{-\frac{2}{3}}(\frac{\partial h}{\partial C_{PQ}}C_{IJ}^{-1} - h\frac{\partial C_{IJ}^{-1}}{\partial C_{PQ}})$$

$$\frac{\partial}{\partial C_{PQ}}(2c_{11}(J-1)JC_{IJ}^{-1}) = c_{11}J^2 C_{PQ}^{-1}C_{IJ}^{-1} + 2c_{11}(J-1)(\frac{1}{2}JC_{IJ}^{-1}C_{PQ}^{-1} - J\frac{\partial C_{IJ}^{-1}}{\partial C_{PQ}}) \tag{61}$$

3) $\dfrac{\partial \underline{\mathbf{S}}_0^{E}}{\partial \underline{\mathbf{C}}}$

$$\frac{\partial S_{0IJ}^E}{\partial C_{PQ}} = \frac{\partial}{\partial C_{PQ}}(C_{IK}^{-1}E_{0K}D_{0J} - \frac{1}{2}\kappa_0 J E_{0K}C_{KM}^{-1}E_{0M}C_{IJ}^{-1}) \tag{62}$$

$$D_{0J} = \kappa_0(J + \kappa_r)C_{JM}^{-1}E_{0M} \tag{63}$$

$$\frac{\partial S_{0IJ}^E}{\partial C_{PQ}} = \frac{\partial}{\partial C_{PQ}}(\kappa_0(J + \kappa_r)C_{IK}^{-1}E_{0K}C_{JM}^{-1}E_{0M} - \frac{1}{2}\kappa_0 J E_{0K}C_{KM}^{-1}E_{0M}C_{IJ}^{-1}) \tag{64}$$

$$\frac{\partial S_{0IJ}^E}{\partial C_{PQ}} = \kappa_0 E_{0K}E_{0M}(\frac{\partial}{\partial C_{PQ}}((J + \kappa_r)C_{IK}^{-1}C_{JM}^{-1}) - \frac{1}{2}\frac{\partial}{\partial C_{PQ}}(JC_{KM}^{-1}C_{IJ}^{-1})) \tag{65}$$

$$\begin{aligned}
\frac{\partial S_{0IJ}^E}{\partial C_{PQ}} &= \kappa_0 E_{0K}E_{0M}(\frac{\partial(J + \kappa_r)}{\partial C_{PQ}}C_{IK}^{-1}C_{JM}^{-1} + (J + \kappa_r)\frac{\partial C_{IK}^{-1}}{\partial C_{PQ}}C_{JM}^{-1} \\
&\quad + (J + \kappa_r)C_{IK}^{-1}\frac{\partial C_{JM}^{-1}}{\partial C_{PQ}} - \frac{1}{2}(\frac{\partial J}{\partial C_{PQ}}C_{KM}^{-1}C_{IJ}^{-1} \\
&\quad + J\frac{\partial C_{KM}^{-1}}{\partial C_{PQ}}C_{IJ}^{-1} + JC_{KM}^{-1}\frac{\partial C_{IJ}^{-1}}{\partial C_{PQ}}))
\end{aligned} \tag{66}$$

$$\begin{aligned}
\frac{\partial S_{0IJ}^E}{\partial C_{PQ}} &= \kappa_0 E_{0K}E_{0M}(\frac{1}{2}JC_{PQ}^{-1}C_{IK}^{-1}C_{JM}^{-1} + (J + \kappa_r)(-\frac{1}{2}(C_{IP}^{-1}C_{KQ}^{-1} + C_{IQ}^{-1}C_{KP}^{-1}))C_{JM}^{-1} \\
&\quad + (J + \kappa_r)C_{IK}^{-1}(-\frac{1}{2}(C_{JP}^{-1}C_{MQ}^{-1} + C_{JQ}^{-1}C_{MP}^{-1})) - \frac{1}{2}(\frac{1}{2}JC_{PQ}^{-1}C_{KM}^{-1}C_{IJ}^{-1} \\
&\quad + J(-\frac{1}{2}(C_{KP}^{-1}C_{MQ}^{-1} + C_{KQ}^{-1}C_{MP}^{-1}))C_{IJ}^{-1} + JC_{KM}^{-1}(-\frac{1}{2}(C_{IP}^{-1}C_{JQ}^{-1} + C_{IQ}^{-1}C_{JP}^{-1}))))
\end{aligned} \tag{67}$$

4) $\frac{\partial \mathbf{S}_0^E}{\partial \mathbf{E}_0}$

$$\frac{\partial S_{0IJ}^E}{\partial E_{0P}} = \frac{\partial}{\partial E_{0P}}(C_{IK}^{-1}E_{0K}D_{0J} - \frac{1}{2}\kappa_0 J E_{0K}C_{KM}^{-1}E_{0M}C_{IJ}^{-1}) \tag{68}$$

$$D_{0J} = \kappa_0(J + \kappa_r)C_{JM}^{-1}E_{0M} \tag{69}$$

$$\frac{\partial S_{0IJ}^E}{\partial E_{0P}} = \frac{\partial}{\partial E_{0P}}(\kappa_0(J + \kappa_r)C_{IK}^{-1}E_{0K}C_{JM}^{-1}E_{0M} - \frac{1}{2}\kappa_0 J E_{0K}C_{KM}^{-1}E_{0M}C_{IJ}^{-1}) \tag{70}$$

$$\begin{aligned}
\frac{\partial S_{0IJ}^E}{\partial E_{0P}} &= \kappa_0(J + \kappa_r)C_{IK}^{-1}C_{JM}^{-1}(\delta_{KP}E_{0M} + E_{0K}\delta_{MP}) \\
&\quad - \frac{1}{2}\kappa_0 J C_{KM}^{-1}C_{IJ}^{-1}(\delta_{KP}E_{0M} + E_{0K}\delta_{MP})
\end{aligned} \tag{71}$$

$$\begin{aligned}
\frac{\partial S_{0IJ}^E}{\partial E_{0P}} &= \kappa_0(J + \kappa_r)(C_{IP}^{-1}C_{JM}^{-1}E_{0M} + C_{IK}^{-1}C_{JP}^{-1}E_{0K}) \\
&\quad - \frac{1}{2}\kappa_0 J C_{IJ}^{-1}(C_{PM}^{-1}E_{0M} + E_{0K}C_{KP}^{-1})
\end{aligned} \tag{72}$$

$$\frac{\partial S_{0IJ}^E}{\partial E_{0P}} = C_{IP}^{-1}D_{0J} + C_{JP}^{-1}D_{0I} - \frac{J}{J + \kappa_r}C_{IJ}^{-1}D_{0P} \tag{73}$$

5) $\dfrac{\partial \underline{\mathbf{D}}_0}{\partial \underline{\mathbf{C}}}$

$$\frac{\partial D_{0I}}{\partial C_{PQ}} = \frac{\partial}{\partial C_{PQ}} \kappa_0 (J + \kappa_r) C_{IJ}^{-1} E_{0J} \tag{74}$$

$$\frac{\partial D_{0I}}{\partial C_{PQ}} = \frac{\partial}{\partial C_{PQ}} (\kappa_0 (J + \kappa_r)) C_{IJ}^{-1} E_{0J} + \kappa_0 (J + \kappa_r) \frac{\partial C_{IJ}^{-1}}{\partial C_{PQ}} E_{0J} \tag{75}$$

$$\frac{\partial D_{0I}}{\partial C_{PQ}} = \frac{1}{2} \kappa_0 J C_{PQ}^{-1} C_{IJ}^{-1} E_{0J} - \frac{1}{2} \kappa_0 (J + \kappa_r) (C_{IP}^{-1} C_{JQ}^{-1} + C_{IQ}^{-1} C_{JP}^{-1}) E_{0J} \tag{76}$$

$$\frac{\partial D_{0I}}{\partial C_{PQ}} = \frac{J}{2(J + \kappa_r)} C_{PQ}^{-1} D_{0I} - \frac{1}{2} D_{0Q} C_{IP}^{-1} - \frac{1}{2} D_{0P} C_{IQ}^{-1} \tag{77}$$

6) $\dfrac{\partial \underline{\mathbf{D}}_0}{\partial \underline{\mathbf{E}}_0}$

$$D_{0I} = \kappa_0 (J + \kappa_r) C_{IJ}^{-1} E_{0J} \tag{78}$$

$$\frac{\partial D_{0I}}{\partial E_{0P}} = \frac{\partial}{\partial E_{0P}} (\kappa_0 (J + \kappa_r) C_{IJ}^{-1} E_{0J}) \tag{79}$$

$$\frac{\partial D_{0I}}{\partial E_{0P}} = \kappa_0 (J + \kappa_r) C_{IJ}^{-1} \delta_{JP} \tag{80}$$

$$\frac{\partial D_{0I}}{\partial E_{0P}} = \kappa_0 (J + \kappa_r) C_{IP}^{-1} \tag{81}$$

References

Dorfmann, A.; Ogden, R. W.: Nonlinear electro-elasticity. *Acta Mechanica*, 174, (2005), 167–183.

Dorfmann, A.; Ogden, R. W.: Nonlinear electroelastic deformations. *J. Elasticity*, 82, (2006), 99–127.

Dorfmann, A.; Ogden, R. W.: Nonlinear electroelastostatics: incremental equations and stability. *Int. J. Eng. Sci.*, 48, (2010), 1–14.

Eringen, A. C.: On the foundations of electroelastostatics. *Int. J. Eng. Sci.*, 1, (1963), 127–153.

Maugin, G. A.; Pouget, J.; Drouot, R.; Collet, B.: *Nonlinear Electro-mechanical Couplings*. Wiley, New York (1992).

McMeeking, R. M.; Landis, C. M.: Electrostatic forces and stored energy for deformable dielectric materials. *J. Appl. Mech.*, 72, (2005), 581–590.

Mueller, R.; Xu, B. X.; Gross, D.; Lyschik, M.; Schrade, D.; Klinkel, S.: Deformable dielectrics - optimization of heterogeneities. *Int. J. Eng. Sci.*, 48, (2010), 647–657.

Pao, Y.: Electromagnetic forces in deformable continua. *Mechanics Today*, 4, (1978), 209–305.

Toupin, R.: The elastic dielectric. *J. Rational Mech. Anal.*, 5, (1956), 849–915.

Vu, D. K.; Steinmann, P.: A 2d coupled bem-fem simulation of electro-elastostatics at large strain. *Comput. Methods Appl. Mech. Engrg.*, 199, (2009), 1124–1132.

Vu, D. K.; Steinmann, P.; Possart, G.: Numerical modelling of non-linear electro-elasticity. *Int. J. Numer. Meth. Eng.*, 70, (2007), 685–704.

Xu, B. X.; Mueller, R.; Klassen, M.; Gross, D.: On electromechanical stability analysis of dielectric elastomer actuators. *APPLIED PHYSICS LETTERS*, 97, (2010), 162908.

Zhao, X.; Suo, Z.: Method to analyze electro-mechanical stability of dielectric elastomers. *Appl. Phys. Lett.*, 91, (2007), 0611921.

Addresses: Dipl.-Ing. Markus Klassen[1], J. Prof. Dr. Baixiang Xu[2], Prof. Dr.-Ing. Sven Klinkel[3] and Prof. Dr.-Ing Ralf Müller[1].
[1]Institute of Applied Mechanics, TU Kaiserslautern, D-67663 Kaiserslautern.
[2]Institute of Materials Science, TU Darmstadt, D-64287 Darmstadt.
[3]Institute of Structural Mechanics, TU Kaiserslautern, D-67663 Kaiserslautern.
email: mklassen@rhrk.uni-kl.de; xu@mfm.tu-darmstadt.de;
klinkel@rhrk.uni-kl.de; ram@rhrk.uni-kl.de.